




PAPR Reduction Technique for Mobile Communication Systems Using Neural Networks

Bianca S. de C. da Silva , Pedro H. C. de Souza , and Luciano L. Mendes , *Member, IEEE*

Abstract—This work proposes a new solution to reduce the Peak-to-Average Power Ratio (PAPR) in Orthogonal Frequency Division Multiplexing (OFDM) systems using Neural Networks (NNs). The NN leverages a training dataset generated by the Memory-less Continuous Search Algorithm (MCSA), which fine-tunes the NN for attaining a similar PAPR reduction of the MCSA. Compared to traditional techniques such as the Partial Transmit Sequence (PTS), the proposed solution offers superior performance by achieving a PAPR reduction of up to 4 dB. Nevertheless, a significant advantage is that the trained NN presents a lower computational complexity compared to the MCSA, without compromising its PAPR reduction capabilities.

Link to graphical and video abstracts, and to code:
<https://latam.ieee9.org/index.php/transactions/article/view/9381>

Index Terms—Neural Network, OFDM, PAPR reduction.

I. INTRODUCTION

THE evolution of mobile communication systems, driven by the popularization of services such as streaming and real-time communication, has resulted in a significant growth in users, but also in a growing scarcity of spectral resources due to the limitations of available frequency bands [1], [2]. To address this challenge, international regulatory agencies, including Anatel in Brazil, have promoted the use of underutilized spectrum, known as TV White Space (TVWS). Brazilian regulations [3], allow the use of idle TV channels in the Very High Frequency (VHF) and Ultra High Frequency (UHF) bands in order to expand Internet services in areas with limited average, as long as there is no interference with primary users [4]. This approach not only helps overcome spectral shortages, but also facilitates digital inclusion in remote regions while promoting more efficient use of available resources [5], [6].

However, in Brazil, the maximum transmission power of the secondary network is limited to 1 W of peak power to guarantee coexistence between primary and secondary users. This restriction can compromise network performance in terms of coverage and efficiency, especially when using multi-carrier waveforms with high Peak-to-Average Power Ratio (PAPR) [7], such as Orthogonal Frequency Division Multiplexing (OFDM) [8]. Although OFDM systems are widely

used in modern communications due to its robustness and high data rates, this waveform presents high PAPR and can cause the RF amplifier to operate in non-linear regions. This results in distortions, Inter-carrier Interference (ICI) and high Out-of-Band Emissions (OOBE) [9], which can degrade signal quality, and interfere with incumbents.

There is a wide range of strategies for meeting the challenge of reducing the PAPR in communication systems available in the literature [?]. The classical PAPR reduction methods in wireless communication systems may be insufficient to address the complex and dynamic nature of this challenge [10]. While these methods may offer some degree of PAPR reduction, they may also lack the necessary flexibility to consistently maintain the signal quality under changing communications environments. On the other hand, Machine Learning (ML) algorithms are now playing a fundamental role in reducing the PAPR in OFDM systems [11], by providing more sophisticated and flexible approaches.

In [12], the use of an autoencoder is proposed for PAPR mitigation in Generalized Frequency Division Multiplexing (GFDM) systems. The evaluation, performed using Complementary Cumulative Distribution Function (CCDF), demonstrated the superiority of the PAPR-Reducing Network (PRnet) method over traditional PAPR reduction approaches, laying the foundation for further explorations in the field of applied neural networks. Similarly, the authors of [13] introduce a real-valued neural network in OFDM systems, integrating PAPR reduction and decompression modules to simultaneously minimize the PAPR and Bit Error Rate (BER) values. The simulations results in [13] showed a significant 3.5-fold reduction in BER with lower computational complexity, demonstrating an improvement over the PRnet. This work paves the way for more efficient solutions in the context of Multiple-Input Multiple-Output (MIMO) systems. Moreover, the work [14] proposes a ML approach called PAPRer, which accurately adjusts PAPR targets in Fifth Generation (5G) systems, with an emphasis on minimizing loss functions to optimize performance and complexity. This approach represents an advance in PAPR target prediction and also attests to the use of supervised learning for fine-tuning critical parameters. Furthermore, [15] presents an adaptive modulation scheme that takes into account the PAPR and improves the OFDM energy efficiency. Using online Deep Learning (DL) to improve efficiency, the method proposed in [15] reduces the PAPR by up to 3 dB when compared to traditional approaches, showing interesting advances in the integration of PAPR with energy efficiency management. Another relevant solution is the Deep Unfolding Network (DUN) introduced by [16], which

The associate editor coordinating the review of this manuscript and approving it for publication was Oscar Mauricio Caicedo (*Corresponding author: Bianca da Silva*).

Bianca da Silva, P. H. C. de Souza, and L. L. Mendes are with National Institute of Telecommunications, Santa Rita do Sapucaí, Brazil (e-mails: bianca.silva@mtel.inatel.br, pedro.carneiro@dtel.inatel.br, and luciano.l@inel.br).

uses deep unfolding for dynamic interval adjustment and PAPR reduction. This solution stands out for its computational efficiency and the ability to control the transmission power, integrating trainable parameters and stochastic optimization algorithms. In contrast, [17] adopts tensor settlement to reduce the number of outages in DL architectures, such as Tensor-train Residual Deep Neural Network (TT-RDNN), promoting the PAPR reduction without compromising the linear response of the power amplifier. This method presents an efficient alternative in terms of memory and training time, with applicability in a variety of modulation alphabets. Finally, [18] focuses on the joint optimization of the transmit and receive filters using ML algorithms, reducing both PAPR and Adjacent Channel Leakage Ratio (ACLR). This method is particularly promising for Sixth Generation (6G) networks since it promotes competitive information rates without increasing the complexity at the transmitter.

Although the aforementioned approaches explore different strategies to mitigate PAPR in OFDM systems, such as the use of autoencoders, deep unfolding, and adaptive modulation, the search for solutions with lower computational complexity remains a central challenge. In this context the Memory-less Continuous Search Algorithm (MCSA) emerges: an exhaustive combinatorial approach that randomly explores a large set of solutions to the problem of PAPR reduction in OFDM systems. Despite being effective, the MCSA can be computationally intensive due to the evaluation of many possible changes.

The main objective of this work is to propose a Neural Network (NN) that achieves a similar performance to the MCSA in terms of PAPR reduction, but with much lower complexity. We use a training dataset generated by the MCSA, containing OFDM signals with different pilot configurations and their resulting PAPR values. During offline training, the NN learns to associate the pilot configurations with their impact on the PAPR. Since the NN fix its parameters after the offline training, it follows that its computational complexity during operation is much lower than that of the MCSA, allowing fast and efficient pilot configurations. It is also important to highlight that a small number of pilots can be used in MCSA, reducing the impact of the proposed method on the overall spectral efficiency of the system. In the example used in this paper for performance evaluation, only two subcarriers were sufficient to achieve the desired PAPR. The performance of the proposed method is then compared with the Partial Transmit Sequence (PTS) method because it is a method commonly used in the literature for comparison.

This paper is structured as follows: Section II offers an overview of the OFDM system followed by the challenges associated with the PAPR reduction, and in the sequence both the PTS and MCSA methods are explained. Section III outlines the proposed NN. Section IV presents the numerical results, focusing on the PAPR, computational complexity, and BER performance metrics. Lastly, Section V concludes the paper and discusses potential future research directions.

A. Notation

In this paper, we adopt the following notational conventions: the element located in the i th row and j th column of the matrix

\mathbf{X} is denoted by $X_{i,j}$. The sets of real and complex numbers are denoted by \mathbb{R} and \mathbb{C} , respectively, and the absolute value of a real number $x \in \mathbb{R}$ or the modulus of a complex number $x \in \mathbb{C}$ is denoted by $|x|$. For vectors of dimension X with real and complex entries, the notations \mathbb{R}^X and \mathbb{C}^X are used. The dimension of a vector \mathbf{x} is expressed as $\dim(\mathbf{x})$, and its transpose, as well as the transpose of a matrix \mathbf{X} , are denoted by \mathbf{x}^T and \mathbf{X}^T , respectively. The Hermitian operator is denoted as $(\cdot)^H$. The expected value of a variable Z is denoted by $\mathbb{E}[Z]$, while the real and imaginary parts of $Z \in \mathbb{C}$ are denoted by $\Re(Z)$ and $\Im(Z)$. The estimates of a scalar x , a vector \mathbf{x} , and a matrix \mathbf{X} are denoted by \hat{x} , $\hat{\mathbf{x}}$, and $\hat{\mathbf{X}}$, respectively. Finally, the computational complexity is described by the asymptotic operator $\mathcal{O}(\cdot)$.

II. OFDM PRINCIPLES

OFDM is a fundamental waveform in wireless communications, using orthogonal subcarriers to transmit M -Quadrature Amplitude Modulation (QAM) modulated symbols [19]. Its main advantages include high spectral efficiency, robustness against multipath and low implementation complexity, due to the use of Fast Fourier Transform (FFT), Inverse Fast Fourier Transform (IFFT) and frequency-domain equalization [20].

In the following sections, we present the main concepts associated with the OFDM system model and the challenges associated with reducing the PAPR.

A. OFDM Communication Chain

In the OFDM transmitter, as illustrated in Fig. 1, the information bits vector $\mathbf{b} = [b_1, b_2, \dots, b_{\mu K}]^T$, $\mathbf{b} \in \mathbb{R}^{\mu K}$, is mapped into a vector of data symbols $\mathbf{s} = [s_1, s_2, \dots, s_K]^T$, $\mathbf{s} \in \mathbb{C}^K$, corresponding to QAM constellation points. Here, $\mu = \log_2 M$ is the number of bits per QAM symbol, M is the modulation order, and K is the number of subcarriers. Therefore, each element of \mathbf{s} represents μ bits of data and modulates a given subcarrier in the set of available orthogonal sub-channels. The transformation from the frequency domain to the time domain is described by the IFFT, that is

$$\mathbf{x} = \mathbf{F}_K^H \mathbf{s}, \quad (1)$$

where \mathbf{x} is the OFDM symbol in the time domain, $\mathbf{F}_K \in \mathbb{C}^{K \times K}$ is the normalized Fourier matrix and $(\cdot)^H$ is the Hermitian operator. The Cyclic Prefix (CP), composed of K_{CP} samples, is introduced into \mathbf{x} , resulting in $\bar{\mathbf{x}} \in \mathbb{C}^{K+K_{CP}}$. The signal $\bar{\mathbf{x}}$ is transmitted across a channel with impulse response $\mathbf{h} \in \mathbb{C}^{N_{CH}}$, resulting in a linear convolution given by

$$\hat{\mathbf{y}} = \mathbf{h} * \bar{\mathbf{x}} + \mathbf{w}, \quad (2)$$

where N_{CH} is the length of the channel impulse response, $\mathbf{w} \in \mathbb{C}^{K+K_{CP}}$ is the Additive White Gaussian Noise (AWGN) with zero mean and variance $\sigma^2 = \frac{N_0}{2} \mathbf{I}$, and for which N_0 is the noise power spectral density in W/Hz.

To recover the data symbols, as shown in Fig. 1, it is necessary to remove the CP. The evaluation of the received OFDM symbol in the frequency domain then becomes

$$\hat{\mathbf{Y}} = \mathbf{F}_K \mathbf{y}_r = \mathcal{H} \mathbf{s} + \mathbf{w}, \quad (3)$$

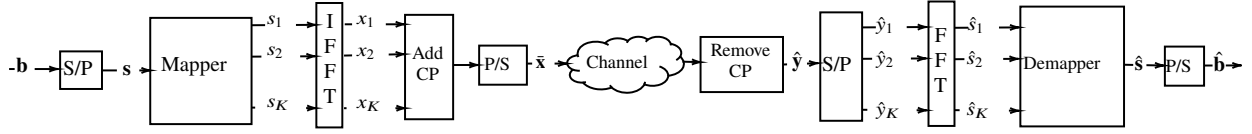


Fig. 1. Transmitter and receiver diagram of the OFDM system.

wherein $\mathbf{w} \in \mathbb{C}^K$ is the AWGN in the frequency domain and $\mathcal{H} = \mathbf{F}_K \mathbf{H} \mathbf{F}_K^H$, $\mathcal{H} \in \mathbb{C}^{K \times K}$, is a diagonal matrix whose main diagonal elements correspond to the frequency response of the channel. The estimate of the transmitted data vector after the equalization in the frequency domain is given by

$$\hat{\mathbf{s}} = \mathbf{s} + \mathcal{H}^{-1} \mathbf{w}, \quad (4)$$

for which $\hat{\mathbf{s}} \in \mathbb{C}^K$. Finally, the estimates of the transmitted bits, $\hat{\mathbf{b}} \in \mathbb{R}^{\mu K}$, can be obtained by implementing the maximum likelihood estimator, for example.

B. PAPR of OFDM Signals

The PAPR is defined as the ratio between the maximum and the average peak powers of the OFDM signal in the time domain [21], that is,

$$\mathcal{P} = \frac{\max(|\mathbf{x}|^2)}{\mathbb{E}[|\mathbf{x}|^2]}. \quad (5)$$

where $\mathbb{E}[\cdot]$ is the expected value of its argument. It is known that the amplitude of the OFDM signal varies approximately according to the noise variation, following a Gaussian distribution. Because the OFDM is a combination of sines and cosines that can occur in phase or counter phase, this results in a large variance in the signal, resulting in power peaks. In other words, there is considerable variation in the amplitude over time, which means that, at certain times, the amplitude can be significantly greater than the Root Mean Square (RMS) value, resulting in a high PAPR [22].

The power peaks of the OFDM signal can drive the power amplifier into saturation, resulting in unwanted clipping of the output signal. These distortions introduce ICI and interference in adjacent channels [23], increasing the OOB. One approach to minimize the PAPR in OFDM systems is to use a large back-off, which significantly reduces the power efficiency of the transmitter. On the other hand, a more efficient approach consists of employing a PAPR reduction technique directly on the OFDM signal, which is used in this work. However, before presenting the proposed method for reducing the PAPR, firstly a the benchmark approaches, namely the PTS and Discrete Fourier Transform (DFT) Spread is described followed by the MCSA details.

C. PTS

In the PTS method, the payload \mathbf{s} is partitioned into D sub-blocks, each subblock being composed of a specific sequence of non-overlapping samples. For example, the first subblock, \mathbf{s}_1 , is composed by the first K/D samples of \mathbf{s} followed by the remaining entries being padded with zeros, while the second subblock, \mathbf{s}_2 , includes the adjacent K/D samples of

\mathbf{s} , preceded and followed by zero padding, and so on. This process ensures that the subblocks are disjoint, meaning that they do not overlap with each other. More precisely, the partitioning can be described as follows

$$\begin{aligned} s_m[i] &= s_i, & (m-1) \frac{K}{D} < i \leq m \frac{K}{D}; \\ s_m[j] &= 0, & j \neq i, \end{aligned} \quad (6)$$

where $s_m[i]$ is an entry of the vector \mathbf{s}_m , $m = \{1, \dots, D\}$ and $K, D \in 2^v$; $v = \{1, 2, 3, \dots\}$ [24].

The IFFT is thus applied separately to each sub-block, resulting in vectors $\mathbf{z}_m = [z_{m,1}, z_{m,2}, \dots, z_{m,K}]^T$, which are then efficiently combined to minimize the PAPR. The main objective is to choose a set of phase arrays that can minimize the PAPR by reducing the probability of several subcarriers being added in phase. Therefore, the output signal is given by [25]

$$\mathbf{z} = \sum_{m=1}^M p_m \mathbf{z}_m, \quad (7)$$

where the phase array is typically defined as [25]

$$p_m = e^{j \frac{2\pi q_m}{u}}, \quad (8)$$

where $0 \leq q_m \leq u-1$ and u is the number of allowed phases. The block diagram presented in [25] illustrates the OFDM transmitter employing the PTS technique.

Finally, at the receiver, the PTS decoding process is performed in reverse to the encoding process. This involves using the same phase arrays used during transmission to recover the original subblocks. Once the subblocks are obtained, they can be combined to reconstruct the original OFDM symbol.

D. DFT Spread

The DFT Spread technique is widely used in the literature to reduce PAPR [26]. Essentially, it consists of adding a FFT to each D sub-blocks in the modulated signal before transmission, followed by the remainder of the conventional OFDM transmitter process. The inclusion of the FFT distributes the signal energy over the subcarriers more evenly, reducing the instantaneous amplitude variation and, consequently, minimizing PAPR.

At the receiver, the reverse process is performed to recover the original data. After the DFT Spread-processed signal has been transmitted, the receiver first applies the conventional FFT of the OFDM system. Then, the IFFT is applied at each sub-blocks to reverse the transformation performed by the FFT at the transmitter. This essential step ensures that the modulated symbols are returned to the time domain prior to demodulation, undoing the previously applied spectrum spreading [27]. As a result, the effect of the DFT Spread is

completely removed at the receiver, ensuring that additional processing does not introduce distortions into the original data.

E. MCSA

MCSA is an exhaustive combinatorial approach that randomly explores a large set of possible solutions without resorting to optimization strategies. In the PAPR reduction scenario, the proposed MCSA is used to randomly select a certain set of pilot subcarriers leading to a PAPR target. The PAPR of each OFDM signal generated with the pilot subcarriers is evaluated and, if it is above a the given target, a new set of pilot subcarriers is drawn. The procedure is repeated until the target PAPR is reached or the maximum number of trials is reached [28].

The pilot allocation operates as follows: after generating the symbol vector, \mathbf{s} , the pilots are then inserted into the symbol. The pilots are the only elements of \mathbf{s} modified in order to achieve the required PAPR. Typically, the position of the pilots is determined by the frame structure of the Radio Access Network (RAN) PHY layer.

The flowchart illustrating the MCSA method employed for PAPR reduction can be found in [28]. For each data vector \mathbf{s} , K_p subcarriers are defined as pilots, which means that the OFDM payload is composed of $K - K_p$ data symbols. Initially, all K_p pilots are set to $\pm\sqrt{E}$, where E is the average energy of \mathbf{s} . The PAPR, \mathcal{P} , of the corresponding OFDM signal is evaluated and compared with a target value \mathcal{P}_{\max} . If the resulting PAPR is below the target, the OFDM signal is transmitted. Otherwise, the OFDM signal is allocated to \mathbf{S}_m , and a new set of random pilots is generated and integrated into the data vector. The PAPR of the new OFDM signal is evaluated and compared again with the target value. This procedure continues until a PAPR below the target value is found or the maximum number of attempts, N_t , is reached. This is necessary to control the system complexity. In this case, the OFDM signal with smaller \mathcal{P} in \mathbf{S}_m is transmitted. Note that the pilot subcarriers do not interfere with the detection procedures.

If the target PAPR is large enough, the MCSA will likely find the set of pilots that meet the criteria with fewer iterations. However, if the target PAPR is considerably lower than the PAPR of a conventional OFDM signal, the number of iterations may increase, which, in turn, increases the overall complexity of the system.

Although the technique proposed in this paper achieves significant PAPR reduction without notably compromising BER performance or spectral efficiency, it necessitates assigning pilot subcarriers for PAPR control. Typically, alterations to the transmission chain require adjustments to the technical specifications of wireless communication standards. Consequently, the algorithm introduced here could be a viable solution for emerging systems, such as 6G networks or future iterations of Wi-Fi. Moreover, in standards where reserved tones are part of the OFDM frame, this technique could be implemented while maintaining compatibility with legacy devices. For instance, the reserved tones in the ISDB-T standard could be utilized to decrease PAPR. Similarly, virtual (or null) subcarriers in LTE and 5G networks could also be leveraged for PAPR reduction.

III. NEURAL NETWORK-BASED PAPR REDUCTION TECHNIQUE

Despite the high complexity of MCSA, due to the large number of IFFTs runs until the pilot set is found, as discussed previously, this approach can be used to create a labeled dataset, where the input is the data symbol vector and the output is the OFDM payload, with pilot subcarriers embedded in the designated positions. This dataset can then be used to train a NN, capable of generating pilot values that achieve the desired PAPR, with low computational cost. This is the approach that this paper presents.

To facilitate understanding of the training, it will be divided into the following steps: (i) Input and output of the NN; (ii) Training of the NN; and (iii) Computational Complexity.

A. Input and Output of the NN

The dataset is composed of N rows and K columns, where each row represents a OFDM symbol transmitted on the MCSA with K subcarriers. In other words, the dataset is the composition of all N symbols transmitted on the MCSA, with the PAPR reduced to the target value \mathcal{P}_{\max} . Furthermore, the dataset is synthetic, that is, it was generated from random numbers within the simulation environment itself.

The proposed NN receives as input the dataset with the positions of the pilot subcarriers set to zero, represented by $\mathbf{S} \in \mathbb{C}^{N \times K}$. During training, the desired output is the dataset where these pilot positions were filled with the values previously calculated in MCSA, denoted by $\mathbf{S}_o \in \mathbb{C}^{N \times K}$. The objective of NN is to correctly predict the values of the originally zeroed pilot subcarriers, having as reference the expected output \mathbf{S}_o .

B. Training of the NN

Before starting the training procedure, it is necessary to rewrite the input as the concatenation of its real and imaginary parts, resulting in $\tilde{\mathbf{S}} \in \mathbb{C}^{N \times 2K}$. This is necessary so that the framework used, TensorFlow, can process the data correctly, since in this case it accepts only real values. Mathematically, this can be described as

$$\tilde{\mathbf{S}} = [\Re(\mathbf{S}) \ \Im(\mathbf{S})], \quad (9)$$

where the first K columns correspond to the real part $\Re(\mathbf{S})$, and the remaining K columns correspond to the imaginary part $\Im(\mathbf{S})$. Note that (9) is used only as a means to organize the input feature data of the NN in a convenient format. Additional details about the dataset are provided in Table I. As can be seen in Fig. 2, the NN that is used in this work is a fully connected multilayer perceptron. Therefore, $\tilde{\mathbf{S}}$ is fed to an input layer, $\ell = 0$, called Flatten. This layer is responsible for turning multidimensional data into one-dimensional data, that is, the matrix $\tilde{\mathbf{S}}$ will enter and a vector with $2K$ elements will come out, maintaining the same characteristics of the original data, so that they can be processed properly during training. After that, the data is processed by the hidden layers, $\ell = \{1, 2, \dots, L\}$, and then the output layer provides \mathbf{S}_o .

Hence, the output $y_{n,\ell}$ for the n th neuron of the ℓ th layer can be described as

$$y_{n,\ell} = f_{n,\ell}(\omega_{n,\ell}^T \mathbf{s}_{\ell-1} + \beta_{n,\ell}), \quad (10)$$

where $n \in \{1, \dots, G_\ell\}$, in which G_ℓ is the total number of neurons for the ℓ th layer, $\omega_{n,\ell}$ represents the weight vector, $\beta_{n,\ell}$ is the bias, and $f_{n,\ell}(\cdot)$ describes the activation function, all associated with the n th neuron of layer ℓ .

TABLE I
DATASET SPECIFICATIONS

Parameter	Value
Number of Samples	576,000 Samples
Bits per Sample	64 bits
Dataset Format	Float64
Total size in bytes	5.22 Mbytes
Data Representation	Real values

Dataset Available at:

https://github.com/BiaSabrina/PAPR_Reduction_NN_dataset

In this work a supervised learning approach is used, where a loss function is employed to minimize the error between the predicted and actual results, leading to

$$L(\Omega, \beta) = \frac{1}{N} \sum_{n=1}^N \mathcal{L}(\bar{\mathbf{S}}, \tilde{\mathbf{S}}(\Omega, \beta)), \quad (11)$$

where N represents the number of training samples, $\mathcal{L}(\cdot)$ is the loss function, and Ω and β are the parameters being optimized. More specifically, the loss function employed in this work is the Mean Square Error (MSE):

$$L(\Omega, \beta) = \frac{1}{N} \sum_{n=1}^N \|\bar{\mathbf{S}}_n - \tilde{\mathbf{S}}_n\|^2 \quad (12)$$

where $\|\cdot\|^2$ is the quadratic norm and $\bar{\mathbf{S}}_n$ ($\tilde{\mathbf{S}}_n$) is the n th row of $\bar{\mathbf{S}}$ ($\tilde{\mathbf{S}}$).

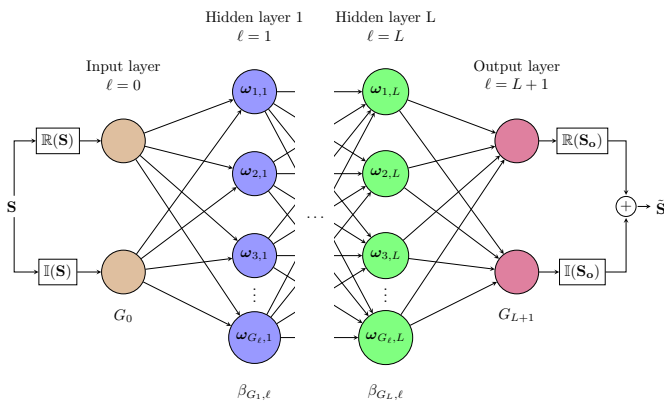


Fig. 2. A neural network architecture consisting of an input layer, hidden layers, and an output layer.

Furthermore, the hyperparameters used in this article can be seen in Table II. One noteworthy hyperparameter is the kernel initialization, for which the Glorot Normal method [29] is used, being also widely adopted in the literature. This method is chosen because it provides an adequate kernel initialization, avoiding excessively high values that could cause

saturation during activation, as well as very low values, which could lead to the problem of gradient vanishing, preventing efficient learning of the network [30]. Moreover, the non-linear activation function used is the Rectified Linear Unit (ReLU), which can be denoted as [31]

$$\text{ReLU}(z_i) = \max(0, z_i), \quad \forall z_i \in \mathbf{z}. \quad (13)$$

TABLE II
NEURAL NETWORK ARCHITECTURE

	Input Layer	Hidden Layer	Output Layer
Number of Neurons	$2K$	500	$2K$
Activation Function	None	ReLU	None
Kernel Initializer	None	Glorot Normal	Glorot Normal
Learning Rate		10^{-3}	
Loss Function		MSE	
Solver		Adam	

C. Computational Complexity

It is possible to estimate the computational complexity of the proposed NN using the flop counting method [32]. As the output of each layer is obtained by (10), the complexity can be expressed by [31]

$$\mathcal{O} \left(\dim(\bar{\mathbf{S}})G_0 + \sum_{\ell=1}^L G_{\ell-1}G_\ell + G_L G_{L+1} \right), \quad (14)$$

where $\dim(\cdot)$ is the size of the input feature data, ℓ is the layer index, and L is the total number of hidden layers. The flop count between the input and the first hidden layer is G_0 , whereas for the last hidden layer connected to the output layer is $G_L G_{L+1}$. For the proposed NN consider that: $G_0 = G_{L+1}$; $\dim(\bar{\mathbf{S}}) = 2K$; $G_0 = 2K$ and $L = 1$. Therefore, (14) can be reduced as follows

$$\mathcal{O}(2K(2K + G_L) + 2K G_L), \quad (15)$$

and further, resulting in

$$\mathcal{O}(K^2 + K G_L). \quad (16)$$

After training the NN only one IFFT is used, in this case, the total complexity of the NN is given by

$$\mathcal{O}(K^2 + K G_L + K \log_2 K), \quad (17)$$

where $K \log_2 K$ is the known complexity of IFFT[33].

IV. NUMERICAL RESULTS AND DISCUSSION

In this section, numerical simulations are used to evaluate the performance of the proposed algorithms. The metrics used in the evaluation are the PAPR, BER, and computational complexity. For the numerical simulation analysis: (i) a 16-QAM OFDM system with 64 subcarriers is considered; (ii) for the MCSA $\mathcal{P}_{\max} = 6$ dB; (iii) two pilot subcarriers are allocated at subcarriers $k = \{1, 62\}$; (iv) $N = 4,500$; and (v) to generate BER the AWGN channel. Moreover, the PTS employs $D = 4$, since this parameter is frequently used in literature [34], and 3,000 epochs for training the NN.

In summary, the NN performed consistently on both training and validation stages. The loss was reduced to 10^{-4} in both stages, as illustrated in Fig. 3. Furthermore, the model accuracy reached 89% on both training and testing data, as shown in Fig. 4, demonstrating that the model generalized well and maintained a good balance between the training and validation stages without overfitting in either cases. Regularization techniques, such as L1/L2 penalties, were tested but did not improve performance, as shown in Fig. 5. In fact, they led to performance degradation, likely due to excessive constraints on the model's ability to capture fine-grained variations necessary for accurate PAPR adjustment.

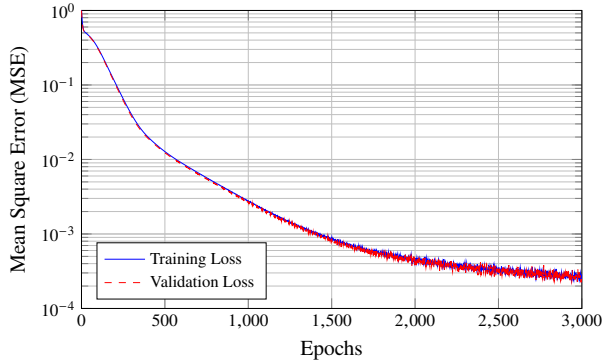


Fig. 3. Loss evaluation for the NN using 3000 epochs.

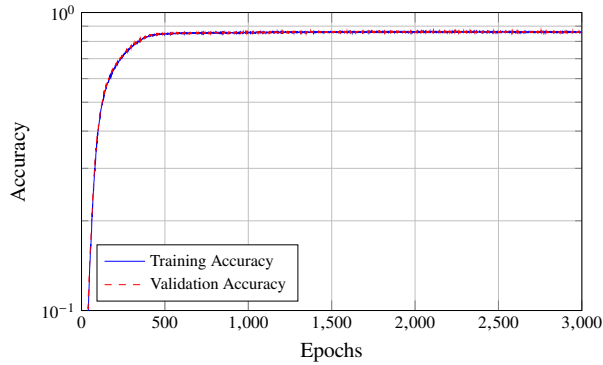


Fig. 4. Accuracy evaluation for the NN using 3000 epochs.

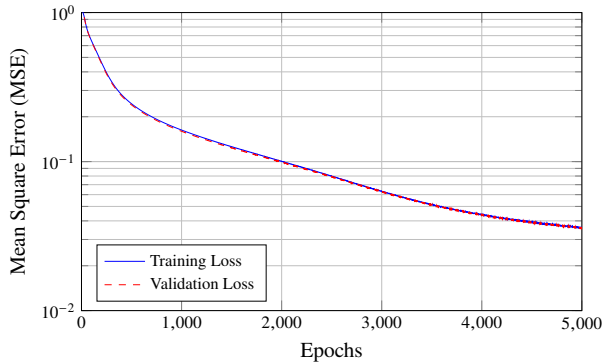


Fig. 5. Loss evaluation for a NN trained over 5000 epochs and regularization technique.

A. PAPR Analysis

Fig. 6 shows the PAPR curves for the MCSA, NN, and the PTS. To better understand CCDF in Fig. 6, it is essential to first define Cumulative Distribution Function (CDF), since one depends on the other. By definition, the CDF of a continuous random variable \mathcal{P} is given by [35]

$$\mathbf{F}_{\mathcal{P}}(P_{thresh}) = P[\mathcal{P} \leq P_{thresh}], \quad -\infty \leq P_{thresh} \leq \infty, \quad (18)$$

where $\mathbf{F}_{\mathcal{P}}(P_{thresh})$ represents the probability that \mathcal{P} assumes a value less than or equal to P_{thresh} .

CCDF, in turn, gives the probability that the random variable \mathcal{P} is greater than a specific value P_{thresh} . Mathematically, CCDF is defined as

$$\bar{\mathbf{F}}_{\mathcal{P}}(P_{thresh}) = 1 - \mathbf{F}_{\mathcal{P}}(P_{thresh}). \quad (19)$$

The PAPR is evaluated using the CCDF, which indicates the probability that the instantaneous power of the signal exceeds a certain value in relation to its average power. This metric is widely used to compare the effectiveness of different PAPR reduction techniques, allowing a clear analysis of the gains obtained by each method.

Fig. 6 illustrates this analysis, highlighting the efficiency of the NN training, evidenced by an MSE of 10^{-4} between the input and output, which demonstrates its high accuracy in preserving the adjusted values. Comparing the methods, it is observed that both MCSA and NN achieve a final PAPR of 6 dB, representing a reduction of 4 dB in relation to the original value. This result significantly surpasses PTS, which achieves only 1 dB of reduction. DFT Spread, although presenting a better performance than PTS, still falls below the proposed methods, MCSA and NN. Although the NN can be seen as a procedure where the reasoning to justify its performance and behavior cannot be explained in a straightforward approach [36], the fact that the NN is trained with a dataset of subcarriers that has been selected to achieve the desired PAPR performance can be considered the main reason for the observed performance. Also, the choice of the hyperparameters of the NN has an important role, since it can impact the probability of underfit or overfit.

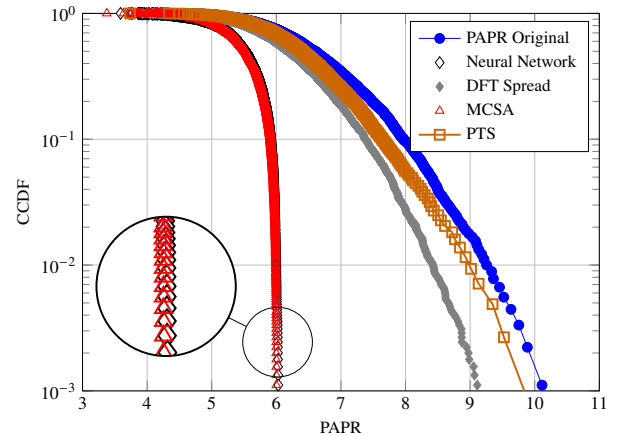


Fig. 6. PAPR for \mathcal{P}_{max} at a level 6 dB.

B. BER Performance Evaluation

The aim of this subsection is to evaluate the impact of the PAPR reduction methods on the BER performance of the OFDM system. For this purpose, all BER curves are obtained considering the AWGN channel. Fig. 7 presents the BER performance for the MCSA, NN, and PTS methods. These results are compared with the theoretical BER, which is given by

$$p_e = \bar{\mu}Q\left(\sqrt{\xi\frac{\epsilon E}{N_0}}\right), \quad (20)$$

where E is the average energy of the QAM constellation, $\bar{\mu} = 4(\sqrt{M} - 1)/\sqrt{M}$ is the average number of symbol neighbors, $\xi = 3/(M - 1)$ is the constellation adjustment factor. The term $\epsilon = (K - K_p)/K$ corresponds to the spectral efficiency adjustment factor of the MCSA and NN. The reduction in spectral efficiency occurs due to the introduction of pilot subcarriers K_p , which do not carry data information.

As illustrated in Fig. 7, both the MCSA method and the NN-based method present a slight degradation in BER performance when compared to the theoretical BER, DFT Spread and the PTS method. This performance degradation can be attributed to the reduction in spectral efficiency caused by the introduction of pilot subcarriers, which reduces the number of useful subcarriers for data transmission. Therefore, this loss in spectral efficiency can be reflected in a reduced transmission power efficiency, since in practice the energy used for transmitting useful data is now being employed in pilot subcarriers for the PAPR reduction.

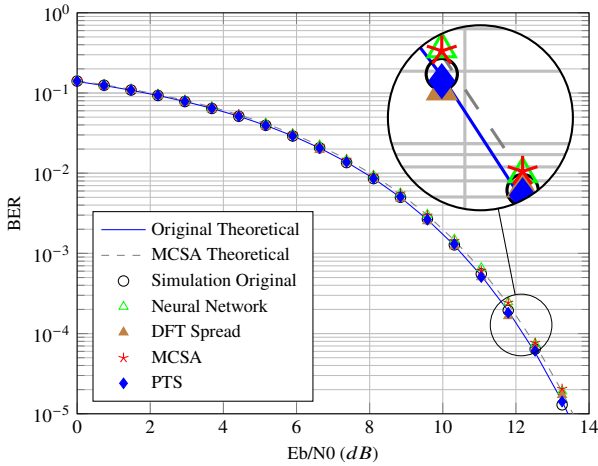


Fig. 7. BER performance over AWGN for the considered PAPR reduction techniques.

C. Complexity Evaluation

The main advantage of the proposed NN method compared to the MCSA method is that the former presents zero variance with respect to the number of IFFT iterations, regardless of the value of \mathcal{P}_{\max} . Variance, in this context, refers to the measure of dispersion or variability in the number of iterations required to achieve a specific target PAPR; a zero variance indicates

that the NN maintains a fixed computational complexity, not varying according to the operating conditions. Moreover, for the MCSA, the average number of iterations is directly related to the value of \mathcal{P}_{\max} and the number of subcarriers. Therefore, a decrease in \mathcal{P}_{\max} , increases the number of subcarriers average computational complexity. This is illustrated in Fig. 8, which presents the averages number of iterations.

Furthermore, it can be assumed that the MCSA average complexity can be given as $O(K^2 \log_2 K)$. This arises from the fact that when the maximum value of the average iteration is reached, as illustrated in Fig. 8, an approximate value of 38 is obtained for $\mathcal{P}_{\max} = 5$ dB and $K = 64$. This result corresponds, on average, to $K/2$ iterations, that is, 32 iterations, a value close to that observed in the Fig. 8. This is due to the need for a larger number of operations to handle the combination of subcarriers in more complex configurations. For a comparison of the complexities between the methods, see Table III, which includes the complexity of NN as evaluated in section III.

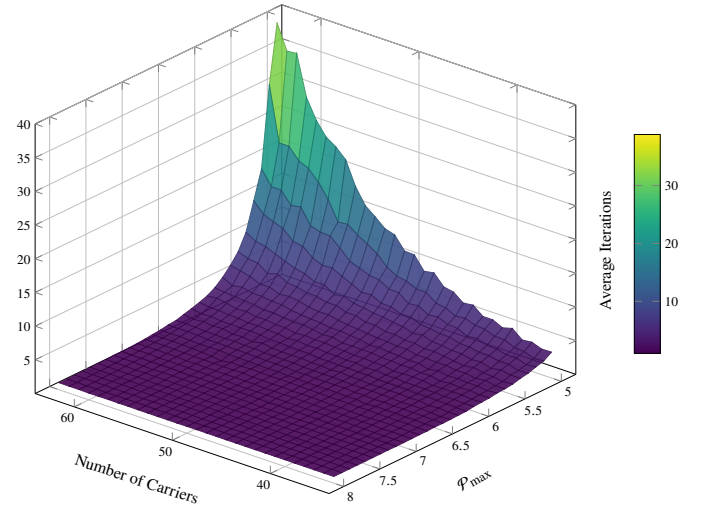


Fig. 8. Average number of iterations for calculating the complexity in terms of IFFTs, compared to \mathcal{P}_{\max} and the number of subcarriers in MCSA.

The NN complexity has as its main component the term K^2 , which represents the highest computational cost, especially in systems with a large number of subcarriers. However, the term KG_L adds to the dominant one, increasing the complexity depending on the number of layers of the NN. Furthermore, after training, only one IFFT is performed on the NN, resulting in adding $K \log_2 K$ in the complexity of this scheme. For the MCSA, the average number of iterations ν term, defines the average number of IFFTs performed to achieve the desired PAPR. It is nevertheless accompanied by a logarithmic term, significantly increasing its computational cost, especially in systems with many subcarriers. Thus, it can be concluded that the complexity of NN is smaller than that of MCSA since NN is not impacted by a logarithmic factor multiplied by ν , as occurs for MCSA. For PTS, we have a constant complexity equal to D . However, it is important to note that MCSA and NN allow reaching a target PAPR, which cannot be done by PTS. The computational complexity of the DFT Spread [37]

remains constant and is given by $K \log_2 K + K \log_2(K/D)$.

TABLE III
COMPUTATIONAL COMPLEXITIES

Method	Complexity
Neural Network	$\mathcal{O}(K^2 + KG_L + K \log_2 K)$
MCSA	$\mathcal{O}(\nu K \log_2 K)$
PTS	$\mathcal{O}(D \cdot K \log_2 K)$
DFT Spread	$\mathcal{O}(K \log_2 K + K \log_2(K/D))$

V. CONCLUSIONS

This work presented a new method to reduce the PAPR in OFDM systems. The proposed method is based on a supervised NN that leverages MCSA as a training dataset. The proposed NN achieves the same performance as MCSA and outperforms PTS, reducing up to 4 dB over the original PAPR. The main advantage of using the NN is the zero-variance complexity for any value of \mathcal{P}_{\max} and number of subcarriers, while for MCSA, the complexity variance varies with \mathcal{P}_{\max} and K . Note that only two pilots were used in MCSA to reduce the impact of the proposed technique on the overall spectral efficiency of the system, and for the purposes of this work, $K_p = 2$ was sufficient to achieve the desired PAPR. Future research topics are the integration of the proposed NN into an OFDM-based transceiver implemented using a software-defined radio approach, to evaluate its performance in a real-world scenario, and the implementation of a new tool to generate the dataset for training the NN according to different standards, such as LTE and 5G-NR.

ACKNOWLEDGMENTS

This work has received partial funding from the project XGM-AFCCT-2024-2-15-1, supported by xGMobile – EM-BRAPII - Inatel Competence Center on 5G and 6G Networks, with financial resources from the PPI IoT/Manufacturing 4.0 program of MCTI grant number 052/2023, signed with EM-BRAPII. Additionally, this work was partially supported by the Ciência por Elas project (APQ-04523-23 funded by Fapemig), the SEMEAR project (22/09319-9 funded by FAPESP), the Brasil 6G project (01245.010604/2020-14 funded by RNP and MCTI), and CNPq-Brasil.

REFERENCES

- [1] N. Rajatheva, I. Atzeni, E. Björnson, A. Bourdoux, S. Buzzi, J.-B. Doré, S. Erkucuk, M. Fuentes, K. Guan, Y. Hu, X. Huang, J. Hultkonen, J. M. Jornet, M. Katz, R. Nilsson, E. Panayirci, K. Rabie, N. Rajapaksha, M. Salehi, and W. Xu, "White Paper on Broadband Connectivity in 6G," *6G Research Visions*, No. 10. University of Oulu, 2020.
- [2] A. Pärssinen, M.-S. Alouini, M. Berg, T. Kuerner, P. Kyösti, M. E. Leinonen, M. Matinmikko-Blue, E. McCune, U. Pfeiffer, and P. Wambacq, "White Paper on RF Enabling 6G – Opportunities and Challenges from Technology to Spectrum," *6G Research Visions*, No. 13. University of Oulu, 2020.
- [3] Anatel, "Resolução nº 190," 2021. [Online]. Available: <https://pesquisa.in.gov.br/imprensa/jsp/visualiza/index.jsp?data=06/10/2021&jornal=515&pagina=25&totalArquivos=181>
- [4] G. P. Villardi, G. Thadeu Freitas de Abreu, and H. Harada, "Tv white space technology: Interference in portable cognitive emergency network," *IEEE Vehicular Technology Magazine*, pp. 47–53, 2012.

- [5] M. Khalil, J. Qadir, O. Onireti, M. A. Imran, and S. Younis, "Feasibility, architecture and cost considerations of using tvws for rural internet access in 5g," in *2017 20th Conference on Innovations in Clouds, Internet and Networks (ICIN)*, 2017, pp. 23–30.
- [6] C.-S. Sum, H. Harada, F. Kojima, Z. Lan, and R. Funada, "Smart utility networks in tv white space," *IEEE Communications Magazine*, pp. 132–139, 2011.
- [7] D. Kong, X. Zheng, Y. Yang, Y. Zhang, and T. Jiang, "A Novel DFT-Based Scheme for PAPR Reduction in FBMC/OQAM Systems," *IEEE Wireless Communications Letters*, vol. 10, no. 1, pp. 161–165, 2021.
- [8] R. van Nee and A. de Wild, "Reducing the peak-to-average power ratio of ofdm," in *VTC '98. 48th IEEE Vehicular Technology Conference. Pathway to Global Wireless Revolution (Cat. No.98CH36151)*, 1998, pp. 2072–2076 vol.3.
- [9] S. J. Shellhammer, A. K. Sadek, and W. Zhang, "Technical challenges for cognitive radio in the tv white space spectrum," in *2009 Information Theory and Applications Workshop*, 2009, pp. 323–333.
- [10] D.-W. Lim, S.-J. Heo, and J.-S. No, "An overview of peak-to-average power ratio reduction schemes for OFDM signals," *Journal of communications and networks*, pp. 229–239, 2009.
- [11] A. Kalinov, R. Bychkov, A. Ivanov, A. Osinsky, and D. Yarotsky, "Machine Learning-Assisted PAPR Reduction in Massive MIMO," *IEEE Wireless Communications Letters*, pp. 537–541, 2021.
- [12] S. Chakravarty and A. Kumar, "PAPR Reduction of GFDM Signals Using Encoder-Decoder Neural Network (Autoencoder)," *National Academy Science Letters*, pp. 213–217, 2023.
- [13] Z. Liu, X. Hu, K. Han, S. Zhang, L. Sun, L. Xu, W. Wang, and F. M. Ghannouchi, "Low-complexity PAPR reduction method for OFDM systems based on real-valued neural networks," *IEEE Wireless Communications Letters*, pp. 1840–1844, 2020.
- [14] S. Gökceli, T. Riihonen, T. Levanen, and M. Valkama, "Machine learning based tuner for frequency-selective PAPR reduction," *IEEE Transactions on Vehicular Technology*, pp. 5378–5383, 2022.
- [15] N. A. Mitsiou, P. D. Diamantoulakis, P. G. Sarigiannidis, and G. K. Karagiannidis, "Energy Efficient OFDM with Intelligent PAPR-aware Adaptive Modulation," *IEEE Communications Letters*, 2023.
- [16] M.-T. Nguyen, G. Kaddoum, B. Selim, K. Srinivas, and P. F. de Araujo-Filho, "Deep Unfolding Network for PAPR Reduction in Multicarrier OFDM Systems," *IEEE Communications Letters*, pp. 2616–2620, 2022.
- [17] M. S. Omar, J. Qi, and X. Ma, "Mitigating Clipping Distortion in Multicarrier Transmissions Using Tensor-Train Deep Neural Networks," *IEEE Transactions on Wireless Communications*, pp. 2127–2138, 2022.
- [18] F. A. Aoudia and J. Hoydis, "Waveform learning for next-generation wireless communication systems," *IEEE Transactions on Communications*, pp. 3804–3817, 2022.
- [19] S. Sun, Y. Ju, and Y. Yamao, "Overlay cognitive radio OFDM system for 4G cellular networks," *IEEE Wireless Communications*, pp. 68–73, 2013.
- [20] Z. Du, N. C. Beaulieu, and J. Zhu, "Selective time-domain filtering for reduced-complexity papr reduction in ofdm," *IEEE Transactions on Vehicular Technology*, pp. 1170–1176, 2009.
- [21] Y. A. Jawhar, L. Audah, M. A. Taher, K. N. Ramli, N. S. M. Shah, M. Musa, and M. S. Ahmed, "A Review of Partial Transmit Sequence for PAPR Reduction in the OFDM Systems," *IEEE Access*, pp. 18 021–18 041, 2019.
- [22] G. Wunder, R. F. Fischer, H. Boche, S. Litsyn, and J.-S. No, "The papr problem in ofdm transmission: New directions for a long-lasting problem," *IEEE Signal Processing Magazine*, pp. 130–144, 2013.
- [23] B. Tang, K. Qin, X. Zhang, and C. Chen, "A clipping-noise compression method to reduce papr of ofdm signals," *IEEE Communications Letters*, pp. 1389–1392, 2019.
- [24] D.-W. Lim, S.-J. Heo, J.-S. No, and H. Chung, "A new pts ofdm scheme with low complexity for papr reduction," *IEEE Transactions on Broadcasting*, pp. 77–82, 2006.
- [25] Y. Rahmatallah and S. Mohan, "Peak-to-average power ratio reduction in ofdm systems: A survey and taxonomy," *IEEE Communications Surveys & Tutorials*, vol. 15, no. 4, pp. 1567–1592, 2013.
- [26] G. Berardinelli, "Generalized dft-s-ofdm waveforms without cyclic prefix," *IEEE Access*, vol. 6, pp. 4677–4689, 2018.
- [27] K. R. Gudimilta, M. S. A. Khan, S. Amuru, and K. Kuchi, "Pre-dft multiplexing of reference signals and data in dft-s-ofdm systems," *IEEE Open Journal of the Communications Society*, vol. 5, pp. 514–525, 2024.
- [28] B. S. C. da Silva, M. B. de Mello, and L. L. Mendes, "Papr reduction technique for mobile communications system based on pattern learning," in *2024 19th International Symposium on Wireless Communication Systems (ISWCS)*, 2024, pp. 1–6.

- [29] S. Dang, J. Tang, J. Li, M. Wen, S. Abdullah, and C. Li, "Combined relay selection enabled by supervised machine learning," *IEEE Transactions on Vehicular Technology*, vol. 70, no. 4, pp. 3938–3943, 2021.
- [30] K. Hiray and K. V. Babu, "A neural network based channel estimation scheme for ofdm system," in *2016 International Conference on Communication and Signal Processing (ICCSP)*. IEEE, 2016, pp. 0438–0441.
- [31] P. H. De Souza, L. L. Mendes, and M. Chafii, "Compressive learning in communication systems: a neural network receiver for detecting compressed signals in ofdm systems," *IEEE Access*, vol. 9, pp. 122 397–122 411, 2021.
- [32] L. A. Pereira, L. L. Mendes, C. J. Bastos-Filho, and A. C. S Jr, "Machine learning-based linearization schemes for radio over fiber systems," *IEEE Photonics Journal*, pp. 1–10, 2022.
- [33] Y.-W. Lin and C.-Y. Lee, "Design of an fft/iff processor for mimo ofdm systems," *IEEE Transactions on Circuits and Systems I: Regular Papers*, vol. 54, no. 4, pp. 807–815, 2007.
- [34] S. H. Han and J. H. Lee, "PAPR reduction of OFDM signals using a reduced complexity PTS technique," *IEEE Signal Processing Letters*, pp. 887–890, 2004.
- [35] D. A. Guimaraes, *Digital transmission: a simulation-aided introduction with VisSim/Comm*. Springer Science & Business Media, 2010.
- [36] A. B. Arrieta, N. Díaz-Rodríguez, J. Del Ser, A. Bennetot, S. Tabik, A. Barbado, S. García, S. Gil-López, D. Molina, R. Benjamins *et al.*, "Explainable artificial intelligence (xai): Concepts, taxonomies, opportunities and challenges toward responsible ai," *Information fusion*, vol. 58, pp. 82–115, 2020.
- [37] M. D. Nisar, H. Nottensteiner, and T. Hindelang, "On performance limits of dft spread ofdm systems," in *2007 16th IST Mobile and Wireless Communications Summit*, 2007, pp. 1–4.



Bianca S. de C. da Silva received the B.S. degree in Control and Automation Engineering in 2020 and the M.Sc. degree in Telecommunications Engineering in 2025, both from the National Institute of Telecommunications (INATEL), Santa Rita do Sapucaí, where she is currently pursuing a Ph.D. degree in Telecommunications Engineering. In 2023, she supported field technicians with remote site integration at Ericsson-INATEL.



Pedro H. C. de Souza received the B.S., M.S. and the Doctor degrees in telecommunications engineering from the National Institute of Telecommunications - INATEL, Santa Rita do Sapucaí, in 2015, 2017 and 2022, respectively; is currently working as a postdoctoral researcher in telecommunications engineering at INATEL, with the support of FAPESP (*Fundação de Amparo à Pesquisa do Estado de São Paulo*). During the year of 2014 he was a Hardware Tester with the INATEL Competence Center - ICC. His main interests are: digital communication

systems, mobile telecommunications systems, 6G, reconfigurable intelligent surfaces, convex optimization for telecommunication systems, compressive sensing/learning, cognitive radio.



Luciano L. Mendes received the B.Sc. and M.Sc. degrees from INATEL, Brazil, in 2001 and 2003, respectively, and the Ph.D. degree from Unicamp, Brazil, in 2007, all in electrical engineering. Since 2001, he has been a Professor with INATEL, where he has acted as the Technical Manager of the Hardware Development Laboratory, from 2006 to 2012. From 2013 to 2015, he was a Visiting Researcher with Vodafone Chair Mobile Communications Systems, Technical University of Dresden, where he had developed his postdoctoral training. In 2017, he was

elected as the Research Coordinator of the 5G Brazil Project, an association involving industries, telecom operators, and academia, which aims for funding and build an ecosystem toward 5G in Brazil. He is the Technical Coordinator of Brazil 6G Project and general coordinator of the XGMobile - Competence Center.